

This is an Open Access document downloaded from ORCA, Cardiff University's institutional repository: <https://orca.cardiff.ac.uk/id/eprint/94840/>

This is the author's version of a work that was submitted to / accepted for publication.

Citation for final published version:

Golkaram, Shirin, Rashidnejad-Omran, Nematollah, Azizi, Hossein, Asahara, Yoshihiro, Buchs, David, McDonald, Iain and Santos, José Francisco 2016. Petrogenesis and geodynamic evolution of the Kajan Neogene subvolcanic rocks, Nain, Central Iran. *Chemie der Erde - Geochemistry* 76 (4), pp. 567-578. 10.1016/j.chemer.2016.08.007

Publishers page: <http://dx.doi.org/10.1016/j.chemer.2016.08.007>

Please note:

Changes made as a result of publishing processes such as copy-editing, formatting and page numbers may not be reflected in this version. For the definitive version of this publication, please refer to the published source. You are advised to consult the publisher's version if you wish to cite this paper.

This version is being made available in accordance with publisher policies. See <http://orca.cf.ac.uk/policies.html> for usage policies. Copyright and moral rights for publications made available in ORCA are retained by the copyright holders.



Petrogenesis and geodynamic implications of the Kajan Neogene subvolcanic, Nain, Central Iran

S. Golkaram^a, N. Rashidnejad–Omran^{a*}, H. Azizi^b, Y. Asahara^c; D. M. Buchs^d, I. McDonald^d,
J. F. Santos^e

^a *Department of Geology, Tarbiat Modares University, Tehran 14115–175, Iran*

^b *Mining Department, Faculty of Engineering, University of Kurdistan, 66177–15175, Sanandaj, Iran*

^c *Graduate School of Environmental Studies, Department of Earth and Environmental Sciences, Nagoya
University, Nagoya, Japan*

^d *School of Earth & Ocean Sciences, Cardiff University, Cardiff, United Kingdom*

^e *Geobiotec, Departamento de Geociências, Universidade de Aveiro, 3810–193 Aveiro,
Portugal*

**Correspondence to rashid@modares.ac.ir*

Abstract

Kajan subvolcanic rocks in the Urumieh-Dokhtar magmatic arc (UDMA), Central Iran, form a Late Miocene-Pliocene shallow-level intrusion. These subvolcanics correspond to a variety of intermediate and felsic rocks, comprising quartz diorite, quartz monzodiorite, tonalite and granite. These lithologies are medium-K calc-alkaline, with SiO₂ (wt. %) varying from 52 % (wt. %) to 75 (wt. %). The major element chemical data also show that MgO, CaO, TiO₂, P₂O₅, MnO, Al₂O₃ and Fe₂O₃ define linear trends with negative slopes against SiO₂, whilst Na₂O and K₂O are positively correlated with silica. Contents of incompatible trace elements (e.g. Ba, Rb, Nb, La and Zr) become higher with increasing SiO₂, whereas Sr shows an opposite behaviour. Chondrite-normalized multi-element patterns show enrichment in LILE relative to HFSE and

troughs in Nb, P and Ti. These observations are typical of subduction related magmas that formed in an active continental margin. The Kajan rocks show a strong affinity with calc-alkaline arc magmas, confirmed by REE fractionation ($\text{LaN/YbN} = 4.5\text{-}6.4$) with moderate HREE fractionation ($\text{SmN/YbN} = 1.08\text{-}1.57$). The negative Eu anomaly ($\text{Eu/Eu}^* < 1$), the low to moderate Sr content (< 400 ppm) and the Dy/Yb values reflect plagioclase and hornblende (+/- clinopyroxene) fractionation from a calc-alkaline melt. Whole-rock Sr and Nd isotope analyses show that the $^{87}\text{Sr}/^{86}\text{Sr}$ initial ratios vary from 0.704432 to 0.705989, and the $^{143}\text{Nd}/^{144}\text{Nd}$ initial ratios go from 0.512722 to 0.512813. All the studied samples have similar Sr-Nd isotopes, indicating an origin from a similar source, with granite samples that has more radiogenic Sr and low radiogenic Nd isotopes, suggesting a minor interaction with upper crust during magma ascent. The Kajan subvolcanic rocks plot within the depleted mantle quadrant of the conventional Sr-Nd isotope diagram, a compositional region corresponding to mantle-derived igneous rocks.

Keywords: Urumieh-Dokhtar magmatic arc (UDMA); magma differentiation; Sr and Nd isotope ratios; calc-alkaline magmas

1. Introduction

The Urumieh–Dokhtar magmatic arc (UDMA), as a testimony of the Zagros orogeny, has been studied by many researchers (e.g. Berberian and Berberian, 1981; Alavi, 2004; Kananian et al., 2014; Yeganehfar 2012; Dargahi et al., 2010; Aghazadeh et al., 2011; Ghorbani et al., 2014; Rezaei-Kahkhaei et al., 2011; Honarmand et al., 2013 and 2014). The UDMA volcanic zone of Schroder (1944) or the Urumieh–Dokhtar magmatic assemblage of Alavi (2004) has been

interpreted to be a subduction related Andean-type magmatic arc that has been active from the Late Jurassic to the present (Berberian and King, 1981; Berberian et al., 1982). Richards (2003a, 2003b, 2015) and Richards et al., (2012) suggested that The Neotethyan ocean opened in the Permian–Early Triassic as the Cimmerian continental fragments (the cores of Turkey, Iran, Tibet, and Indochina) rifted from the northern Gondwana margin and drifted northwards and the UDMA magmatic belt formed by Eocene subduction of southern Neo– Tethyan Ocean beneath the Eurasian plate.

The UDMA is composed of voluminous tholeiitic, calc-alkaline, and K-rich alkaline intrusive and extrusive rocks (with associated pyroclastic and volcanoclastic successions) along the active margin of the Iranian plates with a major magmatic flare-up in Eocene–Oligocene (e.g. Kananian et al., 2014; Moghadam and Stern, 2011; Moghadam et al., 2016). The oldest rocks in the UDMA are calc–alkaline intrusive rocks, which cut across Upper Jurassic formations and are overlain unconformably by Lower Cretaceous fossiliferous limestone (e.g. Dargahi et al., 2010). Volcanic and magmatic activity in this arc reached its maximum during the Eocene with widespread trachybasalt, andesite, and dacite lavas, ignimbrites and tuffs (Alavi, 1980; Berberian and Berberian 1981; Arvin et al., 2007). Intrusive rocks in the UDMA show a large range of lithologies, dominated by granite, but with small amounts of granodiorite, quartz diorite and gabbro. The plutonic rocks are widely distributed and covering more than 65% of the exposed rock units in the UDMA. Previous petrological studies have been focused on the Eocene volcanic–plutonic rocks, but the younger Pliocene-Quaternary subvolcanic bodies are poorly studied. These sub-volcanic bodies are widespread along the UDMA, especially in its central part. Therefore, important testimonies of the final stages of Neotethys closure and collisional tectonics in the area are preserved in these rocks. In this paper, new geochemical characteristics

and Sr–Nd data of the Kajan subvolcanic, from the central part of the UDMA, are presented and discussed.

2. Regional Geology of Kajan area

Kajan area is a part of West Nain area of the central UDMA (Fig. 1). The geology of West Nain has been studied by researchers in the past (e.g. Amidi, 1975; Yeganehfar et al., 2012; Ghorbani et al., 2014). In the Kajan area (Fig. 1), the oldest rock unit is an early to middle Eocene light green tuffaceous and nummulitic limestone (Amidi, 1975). This unit is overlain by a sequence of volcanic and pyroclastic rocks, including basalt, andesite, acidic (rhyolite–dacite) volcanics, tuff breccia, and ignimbrites. The Kajan subvolcanic rocks mainly consist of (micro-) quartz diorite, quartz monzodiorite and granite (Fig. 1, 2). These bodies are shallow-level intrusions, considered to be Late Miocene–Pliocene in age (see the map). Furthermore, in a recent study of Yeganehfar et al., (2012) on magmatic and geodynamic evolution of Urumieh–Dokhtar, based on a comprehensive age data, they reported that the age of the volcanic rock in West Nain area is about 26-18Ma (Figure 1 in Yeganehfar et al., (2012)) and thus West Nain area is young and considered to be Miocene. Thus, based on the work of Yeganehfar et al., (2012), it is possible to attribute to the Kajan subvolcanic rocks, in western Nain area, a Miocene to Pliocene age. This is in agreement with the late Miocene age proposed by Noghreyan and Khodami (2014) for volcanic rocks from Isfahan (i.e. Nain area).

The Kajan rocks differ from the most of plutonic rocks in the UDMA by their more pronounced porphyritic character. The Kajan subvolcanic mainly consists of (micro-) quartz diorite, quartz monzodiorite and granite (Fig. 1). Different types of dikes are found cutting the main intrusive body of the Kajan area (Fig. 2C). The dikes are variable in thickness, from a few centimeters to a

few meters. Some of the Kajan intrusives contain xenoliths, namely of diorite (Fig. 2D), which were incorporated into the granitoids during their intrusion. The geologic importance of the Kajan subvolcanic is to understand the geotectonic evolution of this area in regards to the final stages of the Neotethys subduction and the transition from subduction to

Figure 1

Figure 2

collisional tectonics in the UDMA. Therefore, in this paper, petrological, geochemical and Sr-Nd isotopic information of the Kajan sub-volcanic rocks are used to constrain the magmatic processes involved in their genesis and to try to understand the relationship between the petrogenetic processes and the geodynamic situation of the Kajan area at the time of those intrusive events. This further to test whether these various rocks are co-genetic, and to investigate the magmatic fractionation and magma mixing processes between basaltic and felsic magmas. Therefore, the main objectives of the present work are: (1) to describe the systematic mineralogical and geochemical variations of the whole rock units; (2) to constrain sources of the end-member magmas; (3) to investigate the petrogenesis of the main rock types; (4) to discuss emplacement mechanisms of shallow-level calc-alkaline plutons in convergent plate boundary setting. It should be pointed that Mineral Chemistry would deeply improve the discussion and comprehension of whole rock- and isotope- geochemistry. Nonetheless, it has been widely demonstrated (e.g. Kananian et al., 2014; Arjmandzadeh et al., 2011) that geochemistry is a stand alone constraint of genesis and evolution of magmas.

3. Petrography

The Kajan intermediate– felsic subvolcanic rocks are medium to fine grained and have granular and porphyritic with microgranular groundmass textures. Studied samples, throughout a chemical classification diagram (see next section) could be classified as quartz-diorite, quartz-monzodiorite, tonalite and granite.

3.1. Quartz diorite

The quartz diorite samples have granular and porphyritic. The later also contains microgranular groundmass textures. The samples shows variations in the proportions of plagioclase (50– 60%), quartz (15–20%), hornblende (5–10%), biotite (5–10%), and K–feldspar (1–5%). Plagioclase (oligoclase– andesine) forms a touching framework of crystals, where the interstices are filled by quartz (and K–feldspar). Twinning planes in plagioclase extend to the edges of the grains, although there is generally a very slight increase of sodium at the rims. There is no correlation between the amounts of biotite and hornblende, although biotite usually dominates. The K–feldspar content increases with increasing biotite. The mafic minerals occur together, however lack of pyroxene in some samples may be due to reactions (and resorption) and replacement with hornblende and biotite with increasing H₂O and decreasing temperature during differentiation. Accessory minerals are titanite magnetite, and zircon (Fig. 3A).

3.2. Quartz monzodiorite

The quartz monzodiorite rocks are typically medium–grained to porphyritic have granular to porphyritic textures. It contains plagioclase (45–55%), K–feldspar (10–20%), quartz (15–20%), hornblende (10–15%), biotite (5–10%), clinopyroxene (0–10%) and opaque minerals (2–3%). Accessory minerals such as titanite and apatite are common in the quartz monzodiorite, where

they occur as euhedral to subhedral grains, either isolated or accompanying biotite. Minor interstitial quartz occurs in regular graphic intergrowth with K-feldspar (Fig. 3B).

3.3. Tonalite

Tonalite contains quartz (20–25), K-feldspar (5–10), plagioclase (40–50), biotite (10–15), hornblende (5–10). The samples are characterized by interstitial quartz, occasional granophyritic intergrowths and biotite–quartz symplectites. Biotite grains are commonly subhedral to euhedral, plagioclase phenocrysts are medium to large, hornblende grains are subhedral to euhedral (Fig. 3C).

3.4. Granite

Granite samples are generally medium-grained. These last textures are characterized by the occurrence of plagioclase phenocrysts. They contain plagioclase (30–35%), K-feldspar (25–30%) and quartz (30–35%), and small proportions of mafic minerals, namely green hornblende (1–5%) and biotite (1–5%). Some of the K-feldspar grains are slightly altered, particularly to clay minerals and occasionally they show micrographic intergrowth with quartz (Fig. 3D). Green hornblende is partially replaced by chlorite and opaque minerals. Magnetite and hematite are the main opaque minerals.

Figure 3

4. Geochemistry

After petrographic studies, a set of 14 samples of the least altered rocks were selected for major and trace elements analysis, by ICP–MS. In addition 10 samples were selected for $^{87}\text{Sr}/^{86}\text{Sr}$ and $^{143}\text{Nd}/^{144}\text{Nd}$ isotopic ratios¹. In this paper to analyse and plot the geochemical data we used GCDkit² software.

4.1. Major and trace elements

In the Kajan subvolcanic, the distribution of the rock compositions may be considered bimodal, one group with SiO_2 contents between 52 and 62 wt% (with only one sample (i.e. K13) having 62 wt % SiO_2) and the other from 70 to 75 wt% (Table 1), leaving a geochemical gap between two groups. However, both groups have sub-alkaline affinity. Figure 4A is the AFM diagram (Irvine and Baragar, 1971) and clearly shows that samples plot in two distinct groups in the calc-alkaline field (Fig. 4A).

Total alkali versus silica (TAS) diagram is widely used for chemical classification of magmatic rocks. This diagram is based on the total alkalis ($\text{Na}_2\text{O}+\text{K}_2\text{O}$) versus SiO_2 (Middlemost, 1994). The Kajan samples plot in the quartz diorite to quartz monzodiorite, tonalite and granite fields. On the K_2O vs. SiO_2 diagram (Fig. 4) of Peccerillo and Taylor, 1976, samples plot in the field of medium-K calc–alkaline rocks. According to the molar A/NK vs. molar A/CNK the intermediate subvolcanic rocks are mainly metaluminous (Fig. 4D), whereas the granites are metaluminous to slightly peraluminous (Fig. 4D).

Table 1

Table 2

¹ The analyses were performed at the University of Nagoya in Japan and University of Cardiff in United Kingdom.

² GeoChemical Data toolkit is free software and can be downloaded from (<http://www.gla.ac.uk/gcdkit>). This is a programme for handling and recalculation of whole-rock analyses from igneous rocks (Janousek et al. 2006). Using GCDkit, the data can be loaded, individual analyses grouped into coherent groups or searched according to various criteria. They can be plotted into commonly used classification diagrams (e.g. Harker plots, TAS, AFM, etc.) as well as a variety of user-defined plots (binary and ternary plots, multiple plots, spider plots) (Janousek et al. 2006).

Figure 4

The Kajan rocks have wide ranges of SiO₂ from 52.4 to 75.3% (see Table 1). According to Fig. 5, in the Harker diagram, Al₂O₃, TiO₂, Fe₂O₃, MgO, MnO, CaO, P₂O₅ decrease with increasing SiO₂, whereas Na₂O and K₂O, increase with increasing SiO₂.

Figure 5

Harker diagrams for selected minor and trace elements (in Fig.6) indicate, with respect to SiO₂ content, a progressive enrichment of both large ion lithophile (e.g. Ba, Rb) and incompatible high field strength (e.g. La, Nb, and Zr) elements opposite to a clear depletion of Sr. Primitive mantle-normalized multi-element diagrams (Fig. 7A) define a relatively similar pattern for all the rock types in the Kajan area. Nonetheless, some differences appear in the relative sizes of the peaks and troughs. The samples mainly display positive Th, K,Pb and Zr, and negative Rb, Ba, and strong negative Nb, P and Ti.

Figure 6

All the samples exhibit similar trace element abundance patterns, with general enrichment in large ion lithophile (LILE) relatively to high field strength elements (HFSE) Chondrite-normalized REE diagram (Nakamura, 1974) is presented in Fig. 7B. This figure shows light-REE enrichment, flat heavy REE (HREE) segments, and significant negative Eu anomalies (except quartz diorite samples). Light-REE enrichment, positive Pb anomaly and the Nb-Ti

troughs on the spider diagram (Fig. 7) are typical of calc-alkaline magmatism in active continental margins (Sun and McDonough, 1989).

Figure 7

4.2. Isotope geochemistry

Ten whole-rock samples ranging from quartz diorite to granite were analyzed for Sr isotope composition (Table 2) and the initial $^{87}\text{Sr}/^{86}\text{Sr}$ ratios fall within the 0.704432 to 0.705989. Four of those samples (three from quartz diorites and one from granite) were also analysed for the Nd isotope composition and the initial $^{143}\text{Nd}/^{144}\text{Nd}$ ratios varies from 0.512722 to 0.512813. All the studied samples have similar Sr-Nd isotopes (Fig. 8), indicating an origin from a similar source, with granite samples that has more radiogenic Sr and low radiogenic Nd isotopes, suggesting a minor interaction with upper crust during magma ascent. The Kajan subvolcanic rocks plot within the depleted mantle quadrant of the conventional Sr-Nd isotope diagram (Fig. 8), a compositional region corresponding to mantle-derived igneous rocks.

Figure 8

Figure 8 also shows that the sample rocks have Sr and Nd isotope composition very similar to those of normal island-arc basalts, suggesting melting in a mantle wedge followed by magmatic differentiation for the basic-intermediate samples. Whereas, granitic sample show enrichment in radiogenic Sr and offset from the mantle array, suggesting that the mantle source was slightly modified either by subduction-derived fluids or melts and/or by continental crust or subducted sediments.

5. Discussion

5.1. Fractional crystallization process

Three petrogenetic scenarios are possible in magmatic systems: (1) closed–system fractional crystallization (e.g. Rezaei-Kahkhaei et al., 2011) (2) assimilation–fractional crystallization (AFC) (e.g. DePaolo, 1981; Spera and Bohrsen, 2001; Thompson et al., 2002; Kuritani et al., 2005) and (3) magma mixing (e.g. Popov et al., 1999; Bea et al., 2005).

The geochemical data for the Kajan subvolcanic suggest that the rocks are I-type, metaluminous subduction-related calcalkaline igneous rocks. The negative correlations between Al_2O_3 , CaO, P_2O_5 , MgO, Fe_2O_3 , MnO, TiO_2 and SiO_2 (Fig. 5) suggest that the rocks are likely the result of fractional crystallization during magmatic evolution, which is also confirmed by the P and Ti depletions and negative Eu anomalies (see also Jamshidi et al., 2015; Moghadam et al., 2016) (Fig. 7).

Normally, negative Eu anomaly, develops with magma differentiation due to fractional crystallization of early Ca-rich plagioclase (Davidson et al., 2013). Quartz-diorite samples do not show a significant Eu anomaly (Fig. 7B); this evidence either suggests that plagioclase was unimportant in the fractionation or a combination of hornblende and plagioclase was involved within the fractionating assemblage in a percentage efficient to suppress the Eu anomaly (e.g. Eyuboglu et al., 2011b; Moghadam et al., 2016; Lucci et al., 2016). These hypotheses could be invoked to explain the lack of a significant Eu anomaly in Kajan quartz-dioritoid rocks. Negative Ti-anomaly is consequence of fractionation of a Ti-rich phase such as Titanite (e.g. Lucci et al., 2016) and/or amphibole (e.g. Tiepolo et al., 2007; Rossetti et al., 2014). A negative variation of Nb/Ta ratio, with respect to SiO_2 enrichment, can indicate a hornblende-controlled fractionation

processes (e.g. Moghadam et al., 2016 and references therein). Moreover, the negative Nb – Ta – Ti anomalies together with positive LREE (La, Ce, Nd and Sm) and Zr anomalies are a typical feature of calc-alkaline arc magmas (e.g. Defant and Drummond, 1990; Martin, 1999). Tectonomagmatic discrimination diagrams (Fig. 9 Pearce et al., 1984) confirm a possible volcanic arc setting characterized by a progressive arc maturity increase from Island Arc to Normal continental arcs (Fig. 10 Brown et al., 1984).

Figure 9

Figure 10

Indication of an important evolution via fractional crystallization processes (FC) can be deduced by both major and trace elements trends with respect to SiO₂ content as differentiation index (Figs. 5 and 6). Progressive depletion of Al₂O₃, MgO, FeO*, CaO, TiO₂, Sr opposite to enrichment of incompatible elements (Na₂O, K₂O, Ba and Rb) clearly suggests a progressive extraction from the melt of crystallized anorthitic plagioclase, hornblende, clinopyroxene and Titanite (e.g. Moghadam et al., 2016) and permanence/enrichment in melt of alkali-feldspar + biotite (e.g. Klimm et al., 2008). Moreover, even if clinopyroxene and hornblende fractionations show similar effects in calc-alkaline magmas, $Cpx-K_D \ll Hbl-K_D$ (e.g. Davidson et al., 2007). Therefore hornblende fractionation is expected to play a major role in the FC-process (Lucci et al., 2016 and references therein).

Increasing of Ba/Sr (Fig. 11A, Klimm et al., 2008) and decreasing of Dy/Yb (Fig. 11B, e.g. Davidson et al., 2007; Rossetti et al., 2014), together with Eu-Ti-Nb-Ta negative anomalies (e.g. Moghadam et al., 2016) point to a fractional crystallization dominated by Pl + Hbl + Ttn ± Cpx,

in agree with the model proposed by Moghadam et al., (2016) and Lucci et al., (2016) for similar calc-alkaline rocks.

Figure 11

5.2. Magma genesis

Three distinct petrogenetic models for magma genesis are discussed to explain the petrological and geochemical features of I-type intrusive rocks: (i) fractionation of mantle-derived magma, (ii) reaction of mantle-derived magma with crustal rocks and (iii) partial melting of crust (Wilson, 2007).

Arc magmas are characterized by a distinct trace element pattern, with LILE enrichment over HFSE, moderate LREE/HREE fractionation and negative anomalies of Nb, Ta and Ti (e.g. Defant and Drummond, 1990; Martin, 1999; Rossetti et al., 2015). There is a general consensus that the described pattern is mainly controlled by fluid and element partitioning from the slab to the mantle wedge (e.g. Tatsumi, 2005; Pichavant and Macdonald, 2007; Zhang et al., 2011).

The Kajan subvolcanic rocks, with negative anomalies in Nb-Ta-Ti-P-Eu and strong enrichment in incompatible elements (e.g. Th, U, K, Rb and LREE), show a strong affinity with calc-alkaline arc magmas, confirmed by REE fractionation ($La_N/Yb_N = 4.5-6.4$) with moderate HREE fractionation ($Sm_N/Yb_N = 1.08-1.57$).

The negative Eu anomaly ($Eu/Eu^* < 1$), the low to moderate Sr content (< 400 ppm) and the Dy/Yb values reflect plagioclase and hornblende (\pm clinopyroxene) fractionation from a calc-alkaline melt (e.g. Moghadam et al., 2016).

The Kajan intermediate rocks shows Sr-Nd isotopic composition very similar to island arc-basalts, implying that Kajan intermediate rocks derived, through magmatic differentiation, by partial melting of the mantle wedge (e.g. Moghadam et al., 2016). The kajan felsic rocks, integrating the bulk geochemistry and Sr-Nd isotopes, instead could represent more differentiated melts that experienced interaction with the crust (e.g. Moghadam et al., 2016).

6. Geodynamic implications

It is generally accepted that the subduction of the Neo-Tethys oceanic lithosphere under the Central Iranian microcontinent continued until the late Oligocene–early Miocene (e.g. Berberian et al., 1982; Ricou, 1994; Mohajjel et al., 2003; Alavi, 2004). The subsequent collision of the major plates resulted in thickening and shortening of the continental crust accompanied by folding, thrusting and uplift of the Iranian plateau (e.g. Ricou, 1994; Moradian–Shahrbabaky, 1997; Mohajjel et al., 2003). The Neogene subvolcanic and granitic rocks of UDMA are the subject of considerable controversy regarding the history and chronology of the Neotethys final closure and of the Arabian– Central Iranian continental collision. The timing of this collision is highly debated most likely due to the lack of precise geochronology; however, it has been inferred that the collision probably took place during Miocene - Pliocene (Berberian and King, 1981).

The contribution of subduction components in the genesis of the Kajan rocks has been shown in a Th/Yb vs. Ta/Yb diagram (Pearce, 1982) (Fig. 12), where the rocks show high Th/Yb content. An increase in the Th/Yb ratio alone is predominantly related to the addition of a subduction-derived component to the arc wedge mantle (Pearce, 1983). The higher Th/Yb ratios of the Kajan

samples could indicate a lithospheric mantle source enriched by subduction components (Dilek et al., 2010).

Figure 12

In a study by Arjmandzadeh and Santos (2014) based on the $\epsilon\text{Ndi}-(^{87}\text{Sr}/^{86}\text{Sr})_i$ diagram they found that their rocks have Sr and Nd isotopic composition very similar to those of normal island-arc basalts, pointing to melting in a mantle wedge followed by magmatic differentiation (Arjmandzadeh and Santos (2014)). Our $\epsilon\text{Ndi}-(^{87}\text{Sr}/^{86}\text{Sr})_i$ diagram (Fig. 13) also shows that the Kajan Intermediate rocks have Sr and Nd isotopic composition very similar to those of normal island-arc basalts.

Figure 13

7. Conclusions

In the present work field observation, petrological, geochemistry and isotopic studies were performed to understand the relationship between the petrogenetic processes and the geodynamic situation of the Kajan subvolcanic rocks in the Urumieh–Dokhtar magmatic arc. The main results of this work are summarized as follows:

- (i) Kajan subvolcanic rocks present intermediate to felsic composition with metaluminous Middle-K calc-alkaline signature, typical of arc magmatism.
- (ii) Whole rock and Sr-Nd isotopic geochemistry both pointed to a co-magmatic origin for the Kajan subvolcanics.

- (iii) Major and Trace elements trends (such as enrichment in LILE and LREE opposite to progressive relative depletion of HFSE and negative anomalies of Eu, Sr, Nb, Ti), moreover, indicate a progressive melt evolution controlled by fractional crystallization processes dominated by progressive extraction of plagioclase + hornblende (+Cpx + Ti-phases).
- (iv) An important contribution of subduction component to the mantle wedge source is recognize throughout Th-Ta-Yb geochemistry in all studied samples, while crust contribution is invocated only for the most evolved felsic rocks as suggested by Sr-Nd isotopic values.

Acknowledgments

The authors gratefully acknowledge Associate Editor Dr. Hadi Shafaii Moghadam from Macquarie University and Dr. Federico Lucci from Università Roma Tre for their constructive comments on the manuscript leading to substantial improvements of the paper.

References

Agard, P., Omrani, J., Jolivet, L., and Mouthereau, F., 2005, Convergence history across Zagros (Iran): Constraints from collisional and earlier deformation: *International Journal of Earth Sciences (Geologische Rundschau)*, 94, 401–419.

Ahmadian, J., Haschke, M., McDonald, I., Regelous, M., Ghorbani, M.R., Emami, M.H., Murata, M., 2009. High magmatic flux during Alpine-Himalayan collision: Constraints from the Kal-e-Kafi complex, central Iran. *Geological Society of American Bulletin* 121, 857–868.

Arjmandzadeh, R., Santos, J. F. 2014. Sr–Nd isotope geochemistry and tectonomagmatic setting of the Dehsalm Cu–Mo porphyry mineralizing intrusives from Lut Block, eastern Iran. *International Journal of Earth Sciences*, 103(1), 123-140.

Arjmandzadeh, R., Karimpour, M.H., Mazaheri, S.A., Santos, J.F., Medina, J.M. and Homam, S.M., 2011. Sr–Nd isotope geochemistry and petrogenesis of the Chah-Shaljami granitoids (Lut block, eastern Iran). *Journal of Asian Earth Sciences*, 41(3), 283-296.

Alavi, M., 1980. Tectonostratigraphic evolution of the Zagrosides of Iran. *Geology* 8, 144-149.

Alavi, M., 2004. Regional stratigraphy of the Zagros fold-thrust belt of Iran and its proforeland evolution. *American Journal of Science* 304, 1-20.

Aghazadeh, M., Castro, A., Badrzadeh, Z., and Vogt, K., 2011, Post-collisional polycyclic plutonism from the Zagros hinterland: The Shaivar Dagh plutonic complex, Alborz belt, Iran: *Geological Magazine*, 148, 980–1008.

Aguillo'n-Robles A., Caimus T., Bellon H, Maury R.C., Cotton J., Bourgois J., Michaud F., 2001. Late Miocene adakites and Nbenriched basalts from Vizcaino Peninsula, Mexico: indicators of East Pacific Rise subduction below southern Baja California. *Geology* 29, 531–534.

Amidi, S.M., 1975. Contribution á létude stratigraphique, pétrologique, et pétrochimique des roches magmatiques de la région de Natanz-Nain-Surk (Iran central). – Thése. Doct. Etat, and F. Grenoble.

Amini, B., and Amini Chehraghi, M.R., 2003. Kajan geological quadrangle map: Iran Geological Survey, scale 1:100 000, 1 sheet.

Arvin, M., Pan, Y., Dargahi, S., Malekizadeh, A., Babaei, A., 2007. Petrochemistry of the Siah-Kuh granitoid stock southwest of Kerman, Iran: implications for initiation of Neotethys subduction. *Journal of Asian Earth Sciences* 30, 474-489.

Batchelor, R.A., Bowden, P., 1985. Petrogenetic interpretation of granitoid rock series using multicationic parameters. *Chemical Geology* 48(1), 43-55.

Bea, F., Fershtater, G.B., Montero, P., Smirnov, V.N., Molina, J. F., 2005. Deformation-driven differentiation of granitic magma: the Stepninsk pluton of the Uralides, Russia. *Lithos* 81(1), 209-233.

Berberian, F., Berberian, M., 1981. Tectono-plutonic episodes in Iran. *Zagros Hindu Kush Himalaya Geodynamic Evolution*, 5-32.

Berberian, F., Muir, I.D., Pankhurst, R.J., Berberian, M., 1982. Late Cretaceous and early Miocene Andean type plutonic activity in northern Makran and central Iran. *Journal of Geological Society of London* 139, 605-614.

Berberian, M., King, G.C.P., 1981. Towards a paleogeography and tectonic evolution of Iran: Reply. *Canadian Journal of Earth Sciences* 18(11), 1764-1766.

Brown, G.C., Thorpe, R.S., Webb, P.C., 1984. The geochemical characteristics of granitoids in contrasting arcs and comments on magma sources. *Journal of the Geological Society* 141(3), 413-426.

Chappell, B.W., 1996. Magma mixing and the production of compositional variation within granite suites: evidence from the granites of southeastern Australia. *Journal of Petrology* 37, 449-470.

Davidson, J., Turner, S., Handley, H., Macpherson, C., Dosseto, A., 2007. Amphibole “sponge” in arc crust?. *Geology* 35(9), 787-790.

Davidson, J., Turner, S. and Plank, T., 2013. Dy/Dy*: variations arising from mantle sources and petrogenetic processes. *Journal of Petrology*, 54(3), 525-537.

Dargahi, S., Arvin, M., Pan, Y., and Babae, A., 2010, Petrogenesis of post-collisional A-type granitoids from the Urumieh– Dokhtar magmatic assemblage, South western Kerman, Iran: Constraints on the Arabian–Eurasian continental collision: *Lithos*, 115, 190–204.

Defant M.J., Jackson T.E., Drummond M.S., De Boer J.Z., Bellon H., Feigenson M.D., Maury R.C., Stewart R.H., 1992. The geochemistry of young volcanism throughout western Panama and southeastern Costa Rica: an overview. *J Geol Soc London* 149, 569–579.

Defant, M.J., Drummond, M.S., 1990. Derivation of some modern arc magmas by melting of young subducted lithosphere. *Nature* 347, 662–665.

DePaolo, D.J., 1981. Trace element and isotopic effects of combined wall rock assimilation and fractional crystallization. *Earth and Planetary Science Letters* 53, 189–202.

Dilek, Y., Imamverdiyev, N., Altunkaynak, S., 2010. Geochemistry and tectonics of Cenozoic volcanism in the Lesser Caucasus (Azerbaijan) and the peri-Arabian region: collision-induced mantle dynamics and its magmatic fingerprint. *International Geology Review* 52, 536–578.

Ghorbani, M.R., Graham, I.T. and Ghaderi, M., 2014. Oligocene–Miocene geodynamic evolution of the central part of Urumieh-Dokhtar Arc of Iran. *International Geology Review*, 56(8), 1039-1050.

Honarmand, M., Omran, N.R., Corfu, F., Emami, M.H. and Nabatian, G., 2013. Geochronology and magmatic history of a calc-alkaline plutonic complex in the Urumieh–Dokhtar Magmatic Belt, Central Iran: zircon ages as evidence for two major plutonic episodes. *Neues Jahrbuch für Mineralogie-Abhandlungen: Journal of Mineralogy and Geochemistry*. 190(1), 67-77.

Honarmand, M., Rashidnejad Omran, N., Neubauer, F., Hashem Emami, M., Nabatian, G., Liu, X., Dong, Y., von Quadt, A. Chen, B., 2014. Laser-ICP-MS U–Pb zircon ages and geochemical and Sr–Nd–Pb isotopic compositions of the Niyasar plutonic complex, Iran: constraints on petrogenesis and tectonic evolution. *International Geology Review*. 56(1), 104-132.

Martin, H., 1999. Adakitic magmas: modern analogues of Archaean granitoids. *Lithos* 46(3), 411-429.

Haschke, M., Siebel, W., Günther, A., Scheuber, E., 2002. Repeated crustal thickening and recycling during the Andean orogeny in north Chile (21–26 S). *Journal of Geophysical Research: Solid Earth* (1978–2012), 107(B1), ECV-6.

Irvine, T., Baragar, W., 1971. A guide to the chemical classification of the common volcanic rocks. *Canadian journal of earth sciences* 8(5), 523-548.

Janousek, V., Farrow, C.M. and Erban, V., 2006. Interpretation of whole-rock geochemical data in igneous geochemistry: introducing Geochemical Data Toolkit (GCDkit). *Journal of Petrology*, 47(6), 1255-1259.

Kananian, A., Sarjoughian, F., Nadimi, A., Ahmadian, J., Ling, W., 2014. Geochemical characteristics of the Kuh-e Dom intrusion, Urumieh–Dokhtar magmatic arc (Iran): implications for source regions and magmatic evolution. *Journal of Asian Earth Sciences* 90, 137-148.

Kay R.W., Kay S.M., 1993. Delamination and delamination magmatism. *Tectonophysics* 219,177–189

Klimm, K., Holtz, F., King, P.L., 2008. Fractionation vs. magma mixing in the wangrah suite A-type granites, Lachlan Fold Belt, Australia: experimental constraints. *Lithos* 102, 415–434.

Kuritani, T., Kitagawa, H., Nakamura, E., 2005. Assimilation and fractional crystallization controlled by transport process of crustal melt: implications from an alkali basalt dacite suite from Rishiri Volcano, Japan. *Journal of Petrology* 46, 1421–1442.

Lucci, F., Rossetti, F., White, J. C., Moghadam, H. S., Shirzadi, A., Nasrabady, M., 2016. Tschermak fractionation in calc-alkaline magmas: the Eocene Sabzevar volcanism (NE Iran). *Arabian Journal of Geosciences*, 9(10), 573. doi:10.1007/s12517-016-2598-0

Mcquarrie, N., Stock, J.M., Verdel, C., and Wernicke, B.P., 2003, Cenozoic evolution of Neotethys and implications for the causes of plate motions: *Geophysical Research Letters*, 30, DOI: 10.1029/2003GL017992.

Middlemost Eric, A.K., 1994. Naming materials in the magma igneous rock system. *Earth Sci. Rev.* 37 (3–4), 215–224

Moghadam, H.S., Stern, R.J., 2011. Geodynamic evolution of Upper Cretaceous Zagros ophiolites: formation of oceanic lithosphere above a nascent subduction zone. *Geological Magazine* 148, 762–801.

Moghadam, Hadi Shafaii, Federico Rossetti, Federico Lucci, Massimo Chiaradia, Axel Gerdes, Margarita Lopez Martinez, Ghasem Ghorbani, and Mohsen Nasrabady., 2016. The calc-alkaline and adakitic volcanism of the Sabzevar structural zone (NE Iran): Implications for the Eocene magmatic flare-up in Central Iran. *Lithos* 248, 517-535.

Mohajjel, M., Fergusson, C.L., Sahandi, M.R., 2003. Cretaceous–Tertiary convergence and continental collision Sanandaj–Sirjan western Iran. *Journal of Asian Earth Sciences* 21, 397–412.

Moradian-Shahrbabaky, A., 1997. Geochemistry, geochronology, and petrology of feldspatoid-bearing rocks in the Urumieh-Dokhtar volcanic belt, Iran. Unpublished Ph. D. thesis, University of Wollongong, Australia, 411.

Nakamura, N., 1974. Determination of REE, Ba, Fe, Mg, Na and K in carbonaceous and ordinary chondrites. *Geochimica et Cosmochimica Acta* 38(5), 757-775.

Noghreyan, M. and Khodami, M., 2014. Magmatic evolution recorded by phenocrysts in volcanic rocks southeast of Isfahan. *Journal of Tethys* 2(1), 55-69.

Pearce, J.A., 1982. Trace element characteristics of lavas from destructive plate boundaries. *Andesites*, 525-548.

Pearce, J.A., 1983. The role of sub-continental lithosphere in magma genesis at destructive plate margins, in Hawkesworth, C.J., and Norry, M.J., eds., *Continental basalts and mantle xenoliths: Nantwich, Shiva*, 230–249.

Pearce, J.A., Harris, N.B. and Tindle, A.G., 1984. Trace element discrimination diagrams for the tectonic interpretation of granitic rocks. *Journal of petrology*, 25(4).956-983.

Pearce, J.A., Bender, J.F., DeLong, S.E., Kidd, W.S., Low, P.J., Guener, Y., Saroglu, F., Yilmaz, Y., Moorbath, S., Mitchell, J.G., 1990. Genesis of collision volcanism in Eastern Anatolia, Turkey. *Journal of Volcanology and Geothermal Research* 44, 189-229.

Peccerillo, A. and Taylor, S.R., 1976. Geochemistry of Eocene calc-alkaline volcanic rocks from the Kastamonu area, northern Turkey. *Contributions to mineralogy and petrology* 58(1), 63-81.

Pichavant, M., and Macdonald, R., 2007. Crystallization of primitive basaltic magmas at crustal pressures and genesis of the calc-alkaline igneous suite: experimental evidence from St Vincent, Lesser Antilles arc. *Contributions to Mineralogy and Petrology* 154(5), 535-558.

Popov, V.S., Tevelev, A.A., Bogatov, V.I., 1999. The Stepninsk pluton on the south Urals: relationships of plutonic rocks coming from mantle and crustal sources. *Izvestiya Vuzov Geologiya i Razvedka Jurnal* 5, 52-68.

Rezaei-Kahkhaei, M., Galindo, C., Pankhurst, R.J. and Esmaeily, D., 2011. Magmatic differentiation in the calc-alkaline Khalkhab–Neshveh pluton, Central Iran. *Journal of Asian earth sciences*, 42(3), 499-514.

Richards, J.P., 2003a, Tectono-magmatic precursors for porphyry Cu-(Mo-Au) deposit formation: *Economic Geology*, v. 98, p. 1515–1533.

Richards, J.P., 2003b. Metallogeny of the Neo-Tethys arc in central Iran. In: Eliopoulos, et al. (Eds.), *Mineral Exploration and Sustainable Development. 7th Biennial SGA Meeting*, Athens, August 24–28. Millpress, Rotterdam, pp. 1237–1239.

Richards, J.P., Spell, T., Rameh, E., Raziq, A., Fletcher, T., 2012. High Sr/Y magmas reflect

arc maturity, high magmatic water content, and porphyry Cu ± Mo ± Au potential: examples from the Tethyan arcs of central and eastern Iran and western Pakistan. *Econ. Geol.* 107, 295–332.

Richards, J. P. 2015. Tectonic, magmatic, and metallogenic evolution of the Tethyan orogen: From subduction to collision. *Ore Geology Reviews* 70, 323–345.

Ricou, L.E., 1994. Tethys reconstructed: plates, continental fragments and their Boundaries since 260 Ma from Central America to South-eastern Asia. *Geodinamica Acta* 7(4), 169-218.

Rollinson, H.R., 1993. *Using Geochemical Data: Evaluation, Presentation, Interpretation.* Longman Scientific & Technical.

Rossetti, F., Nasrabady, M., Theye, T., Gerdes, A., Monié, P., Lucci, F., Vignaroli, G., 2014. Adakite differentiation and emplacement in a subduction channel: the late Paleocene Sabzevar magmatism (NE Iran). *Geological Society of America Bulletin* 126, 317–343.

Rossetti, F., Nozaem, R., Lucci, F., Vignaroli, G., Gerdes, A., Nasrabadi, M., Theye, T., 2015. Tectonic setting and geochronology of the Cadomian (Ediacaran-Cambrian) magmatism in central Iran, Kuh-e-Sarhangi region (NW Lut Block). *Journal of Asian Earth Sciences*, 102, 24-44.

Sajona, F.G., Maury, R.C., Prouteau, G., Cotton, J., Schiano, P., Bellon, H., Fontaine, L., 2000
Slab melt as metasomatic agent in island arc magma mantle sources, Negros and Batan
(Philippines). *Isl Arc* 9,472–486

Schroder, J.W., 1944. Essai sur la structure de l'Iran. *Eclogae Geologicae Helvetiae* 37, 37-81.

Shand, S.J., 1943. *Eruptive Rocks: Their genesis, composition, and classification, with a chapter on meteorites*. J. Wiley & sons, Incorporated.

Spera, F.J., Bohron, W.A., 2001. Energy-constrained open system magmatic processes I: general model and energy-constrained assimilation and fractional crystallization (EC-AFC) formulation. *Journal of Petrology* 42, 999–1018.

Sun, S.S., McDonough, W., 1989. Chemical and isotopic systematics of oceanic basalts: implications for mantle composition and processes. Geological Society, London, *Special Publications* 42(1), 313-345.

Tatsumi, Y., 2005. The subduction factory: how it operates in the evolving Earth. *GSA today*, 15 (7), 4.

Tiepolo, M., Oberti, R., Zanetti, A., Vannucci, R., and Foley, S.F., 2007, Trace-element partitioning between amphibole and silicate melt, in Hawthorne, F.C., Oberti, R., Della Ventura,

G., and Mottana, A., eds., *Amphiboles: Crystal Chemistry, Occurrence and Health Issues: Reviews in Mineralogy and Geochemistry* 67, 417–452.

Thompson, A. B., Matile, L., Ulmer, P., 2002. Some thermal constraints on crustal assimilation during fractionation of hydrous, mantle-derived magmas with examples from central Alpine batholiths. *Journal of Petrology* 43, 403–422.

Whalen, J.B., Jenner, G.A., Longstaffe, F.J., Robert, F. and Gariépy, C., 1996. Geochemical and isotopic (O, Nd, Pb and Sr) constraints on A-type granite petrogenesis based on the Topsails igneous suite, Newfoundland Appalachians. *Journal of Petrology* 37(6), 1463-1489.

Wilson, B.M., 2007. *Igneous petrogenesis a global tectonic approach*. Springer Science & Business Media.

Zhang, X., Mao, Q., Zhang, H., Zhai, M., Yang, Y., and Hu, Z., 2011. Mafic and felsic magma interaction during the construction of high-K calc-alkaline plutons within a metacratonic passive margin: the Early Permian Guyang batholith from the northern North China Craton. *Lithos*, 125(1), 569-591.

Yeganehfar, H., Ghorbani, M. R., Shinjo, R., Ghaderi, M. (2013). Magmatic and geodynamic evolution of Urumieh–Dokhtar basic volcanism, Central Iran: major, trace element, isotopic, and geochronologic implications. *International Geology Review*, 55(6), 767-786.

Figure captions

Fig. 1: A shaded topographic relief map that displays major structural units of Iran (Ahmadian et al., 2009). Simplified geological map of the West Nain area derived, from the geological maps of Kajan (Amini and Amini Chehragh, 2003).

Fig. 2: Field photographs of the Kajan subvolcanic intrusion: A) outcrops of monzodiorite in the western sector of the intrusion; B) sharp contacts between monzodiorite and quartzdiorite; C) dikes cutting the subvolcanic body; D) mafic xenolith enclosed by a granitoid rock.

Fig. 3: Petrographic features of different rocks from the Kajan rocks. A) quartz-diorite, B) quartz-monzodiorite, C) granite, D) syenogranite (granophyric).

Fig. 4: (A) AFM diagram proposed by Irvine and Baragar (1971); (B) Total alkalis vs. silica diagram, with the fields defined by Middlemost, (1994); (C) Plot of K_2O vs. SiO_2 showing subdivision of the calc-alkaline series (Peccerillo and Taylor, 1976); (D) molar A/NK vs. molar A/CNK (Shand 1943), where A, C, N and K are the molar proportions of Al_2O_3 , CaO, Na_2O and K_2O , respectively.

Fig. 5: Harker diagrams for major elements, SiO_2 as differentiation index. Symbols as for figure 4.

Fig. 6: Harker diagrams for selected minor and trace elements. SiO_2 as differentiation index. Symbols as for figure 4.

Fig. 7: (A) Primitive Mantle normalized trace element patterns (Sun and McDonough, 1989) and (B) Chondrite (Nakamura, 1974) normalized REE patterns for Kajan magmatic rocks..

Fig. 8: $^{143}\text{Nd}/^{144}\text{Nd}$ (t) values vs. initial Sr isotopic ratios indicating the source for the magma from the Kajan.

Fig. 9: Rb vs Y+ Nb and Y vs Nb diagrams (Pearce et al. 1984) for Kajan magmatic rocks.

Fig. 10: Rb/Zr vs Nb diagram (Brown et al., 1984) for Kajan magmatic rocks.

Fig. 11: (A) Ba/Sr vs SiO_2 diagram (Rollinson, 1993) and (B) Dy/Yb vs SiO_2 diagram (after Davidson et al., 2007) for Kajan magmatic rocks suggest an evolution via fractional crystallization mainly controlled by plagioclase + hornblende + titanite.

Fig.12: Th/Yb vs. Ta/Yb diagram (Pearce, 1982). A volcanic array from subduction zone is highlighted for Kajan magmatic rocks.

Fig. 13: $\epsilon\text{Nd}_i - (^{87}\text{Sr}/^{86}\text{Sr})_i$ diagram for the Kajan subvolcanic rocks. The field of subducted oceanic crust-derived adakites was defined after Defant et al., (1992), Kay et al., (1993), Sajona et al., (2000) and Aguillón-Robles et al., (2001). MORB: Mid-ocean ridge basalts; DM: Depleted mantle; OIB: Ocean-island basalts; IAB: island arc basalts.

Table captions

Table 1: Bulk rock major and trace elements compositions for Kajan magmatic rocks.

Table 2: Sr-Nd isotope data for Kajan magmatic rocks.

Figures

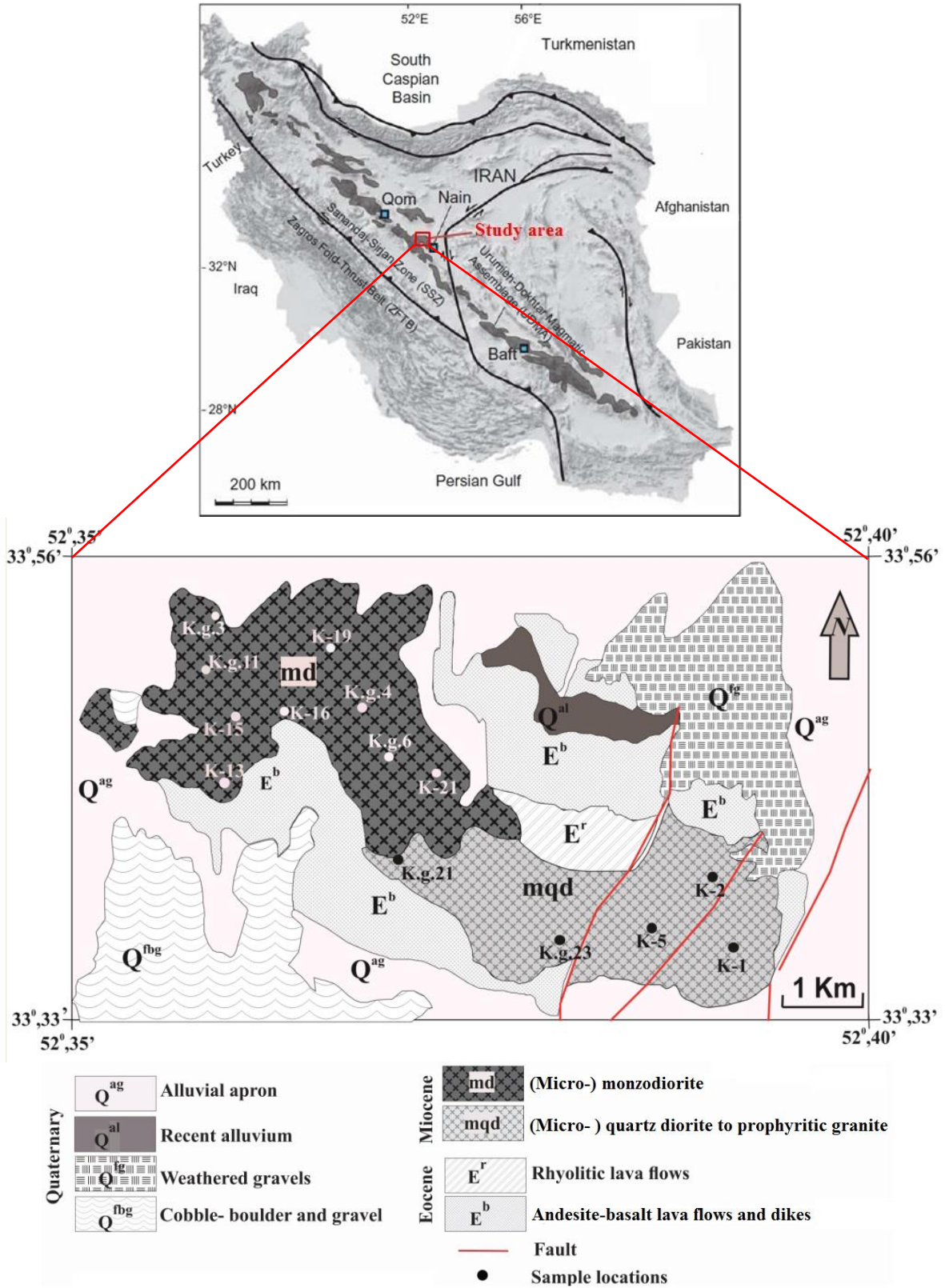


Figure 1

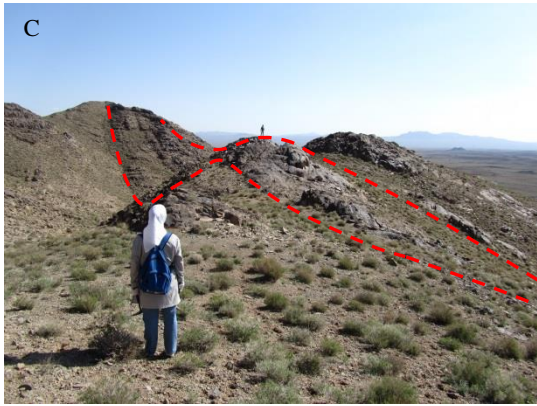


Figure 2

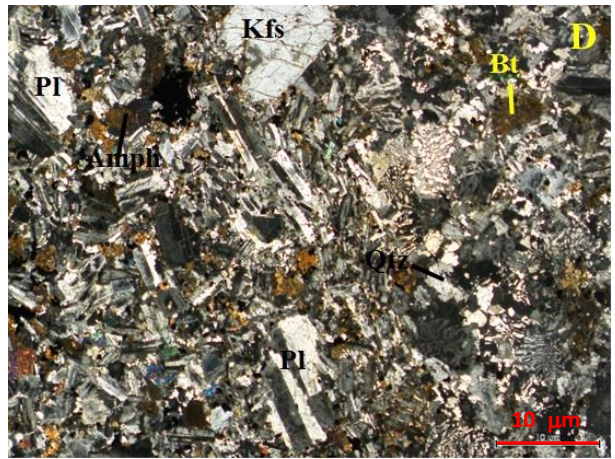
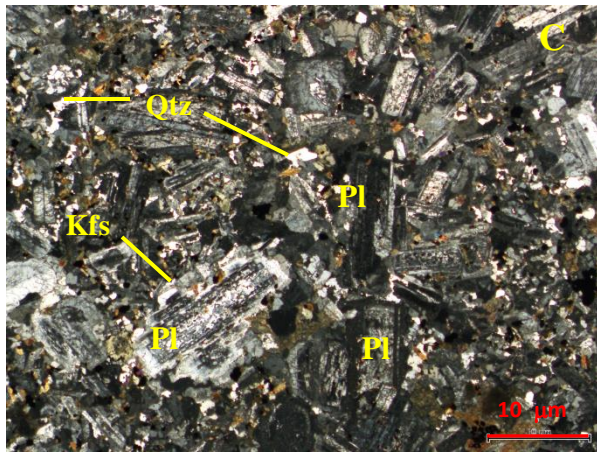
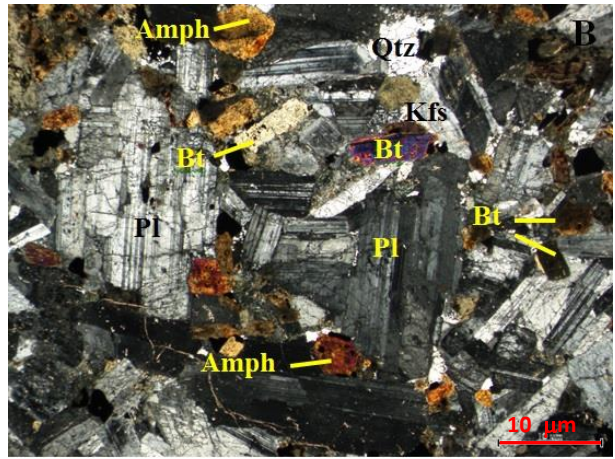
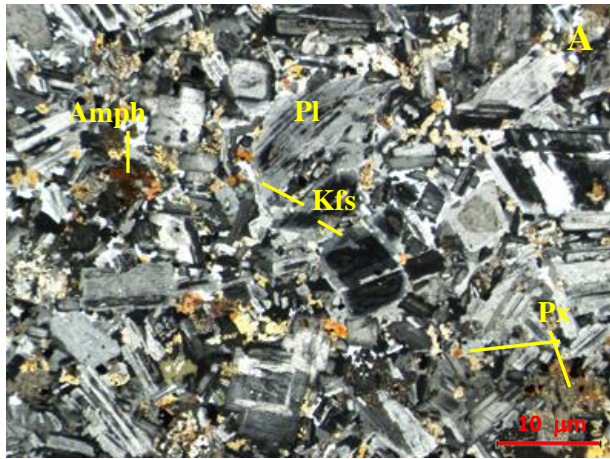


Figure 3

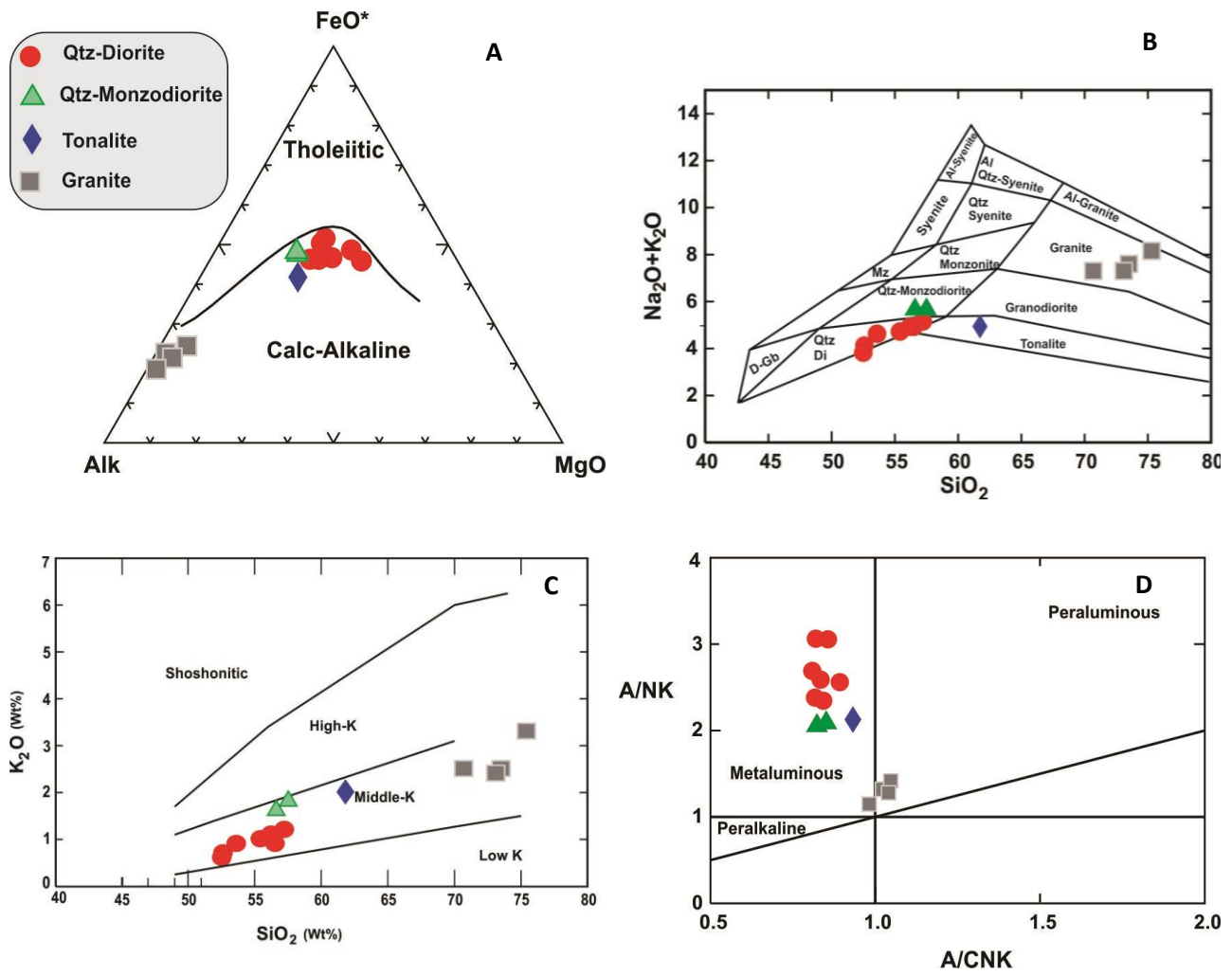
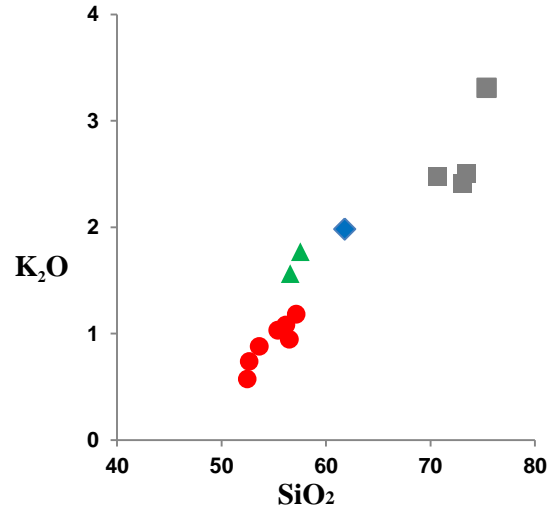
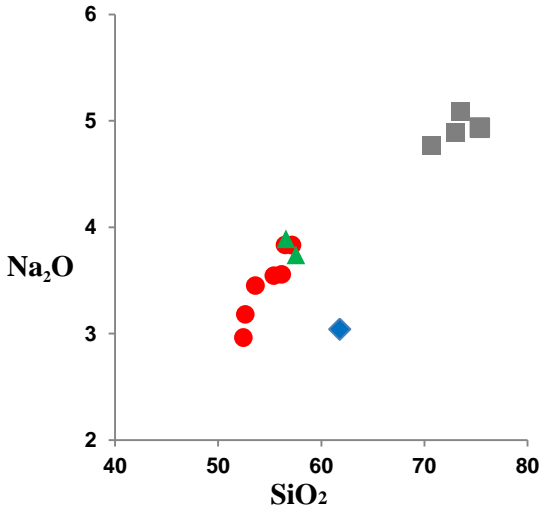
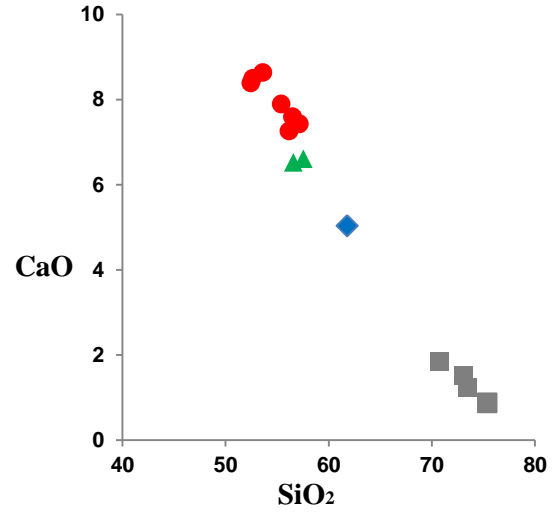
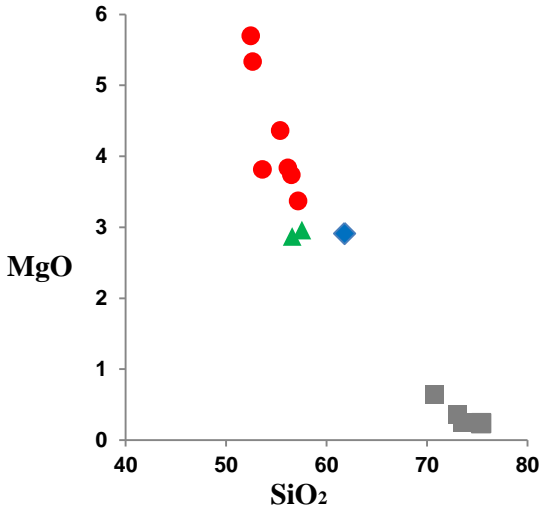
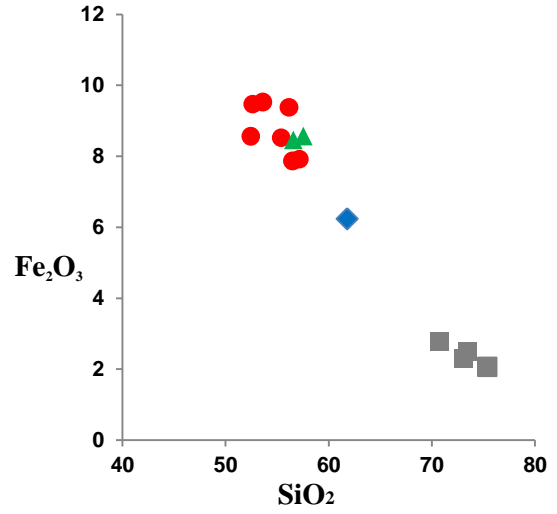
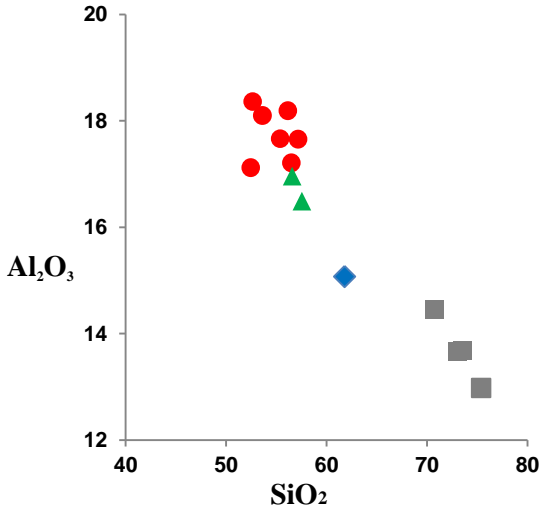


Figure 4



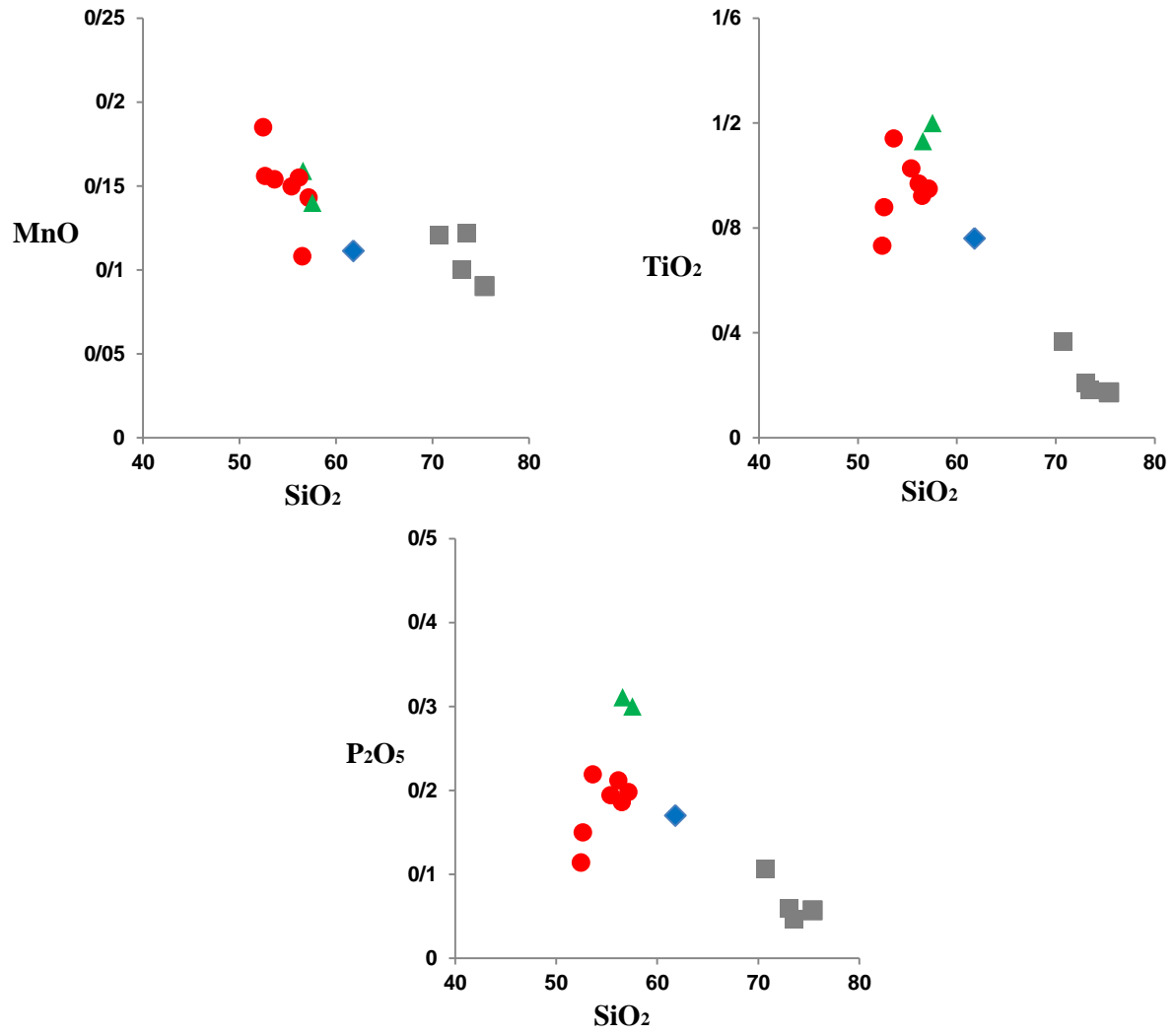


Figure 5

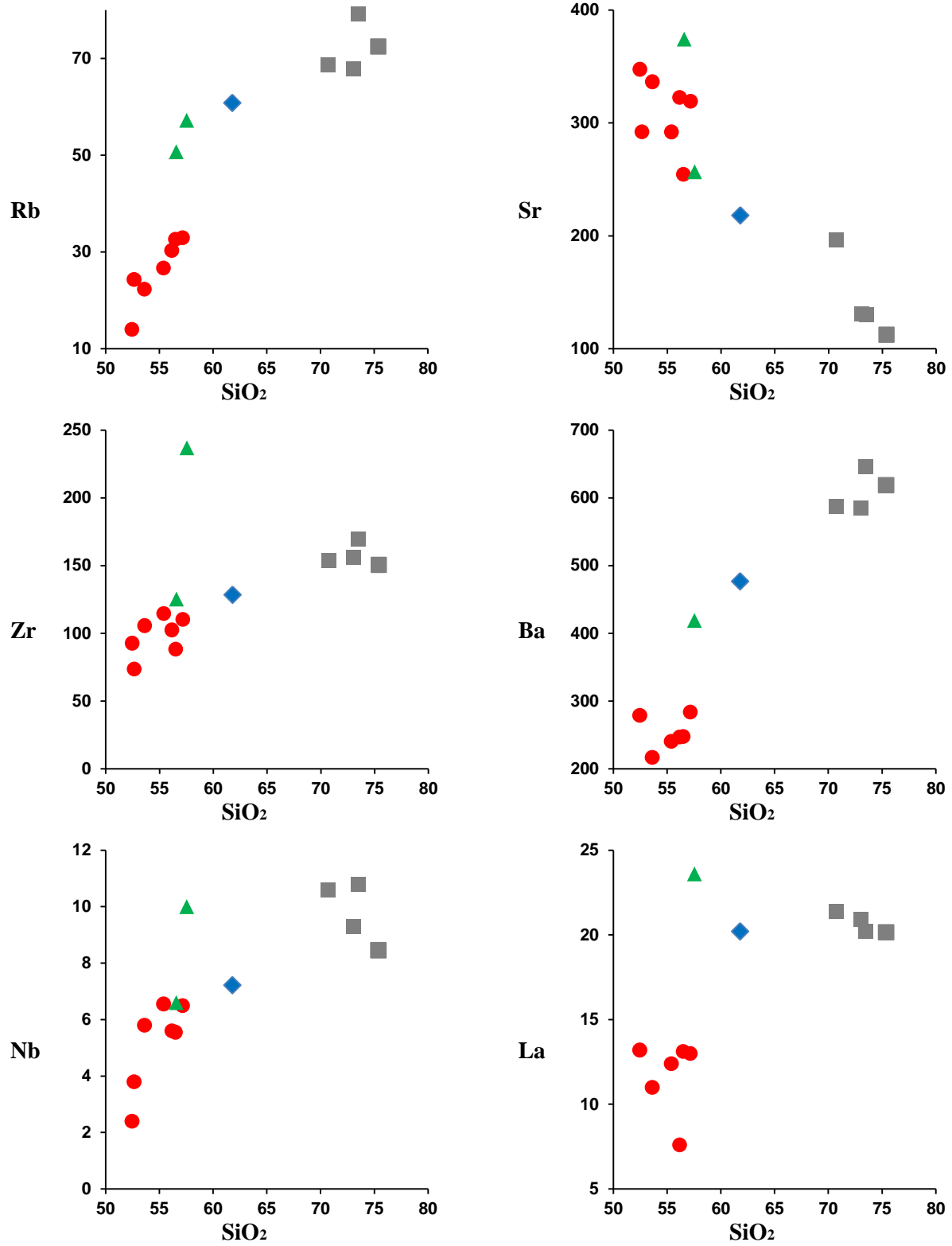


Figure 6

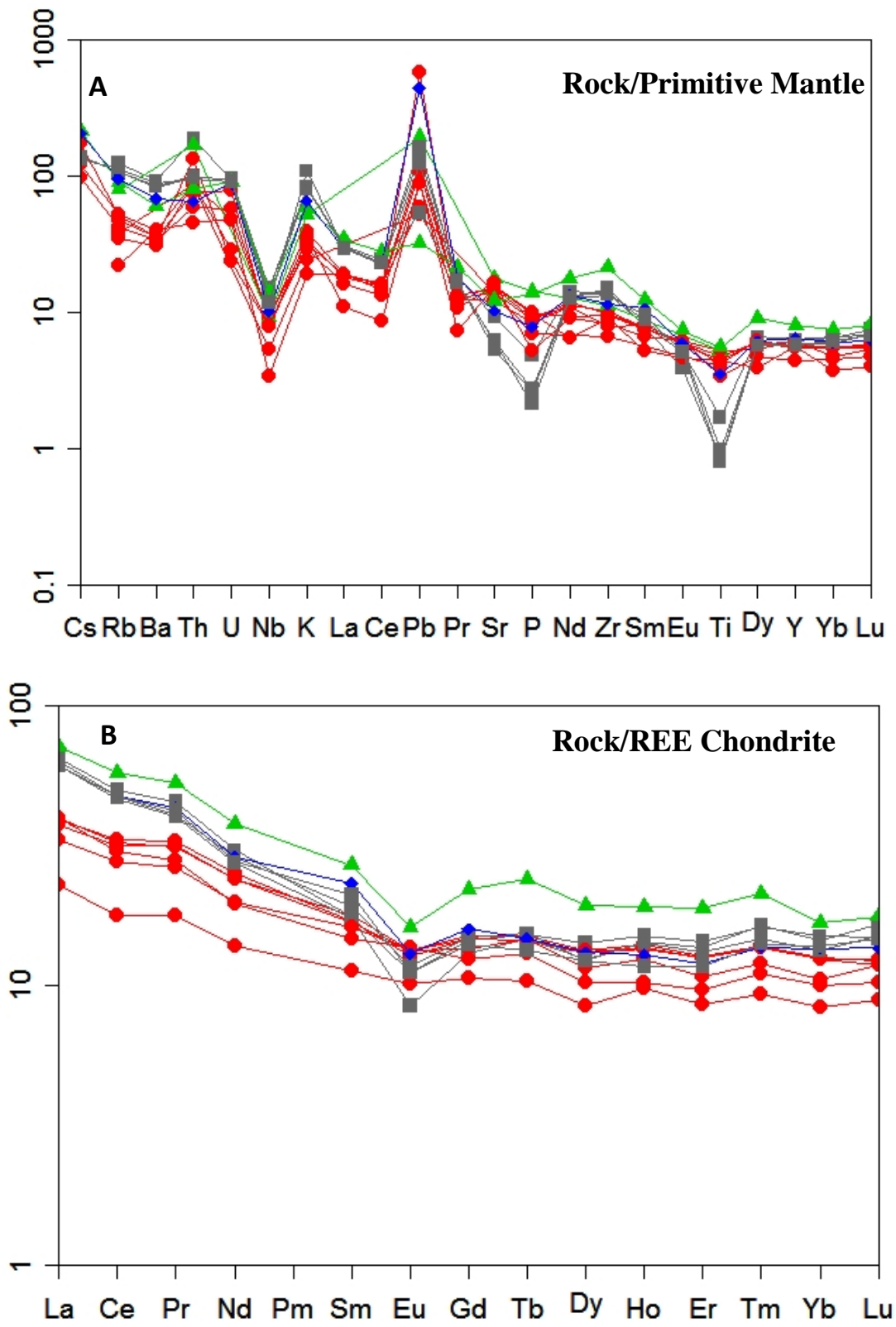


Figure 7

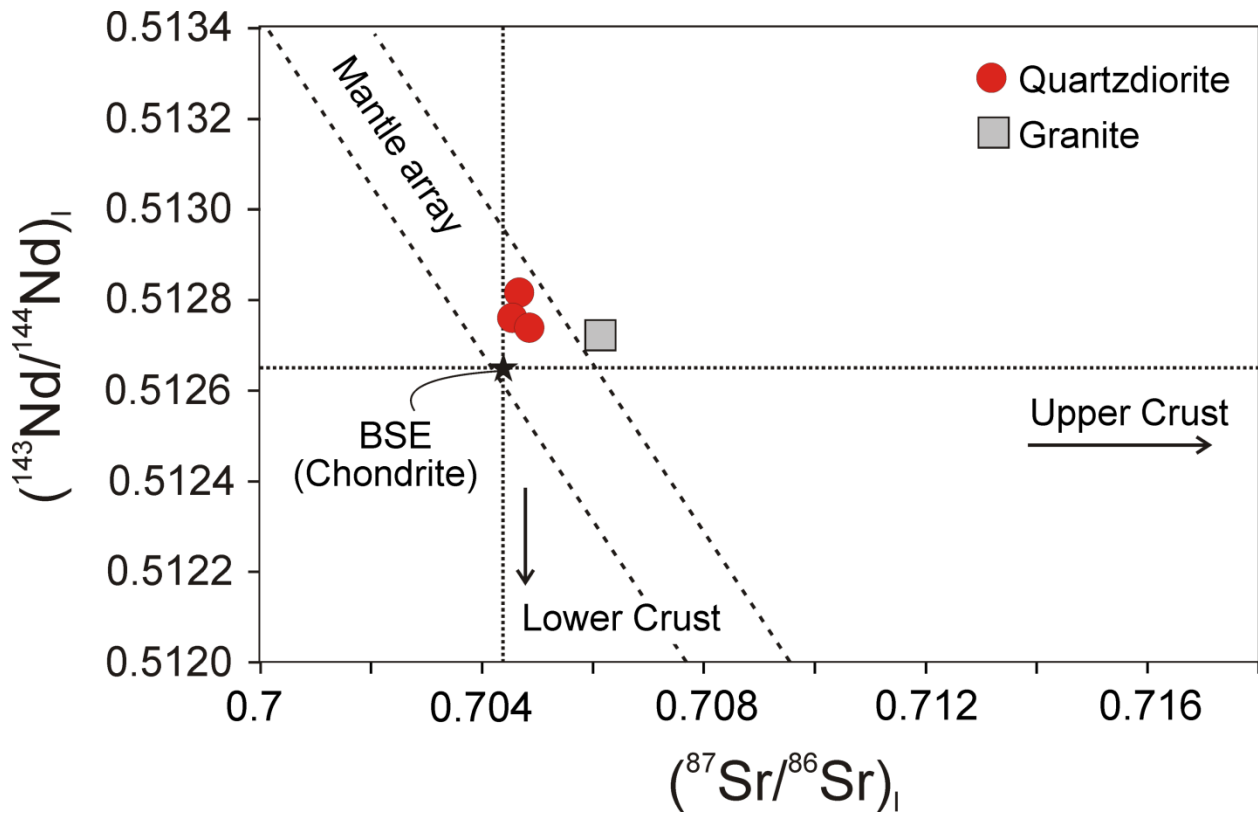


Figure 8

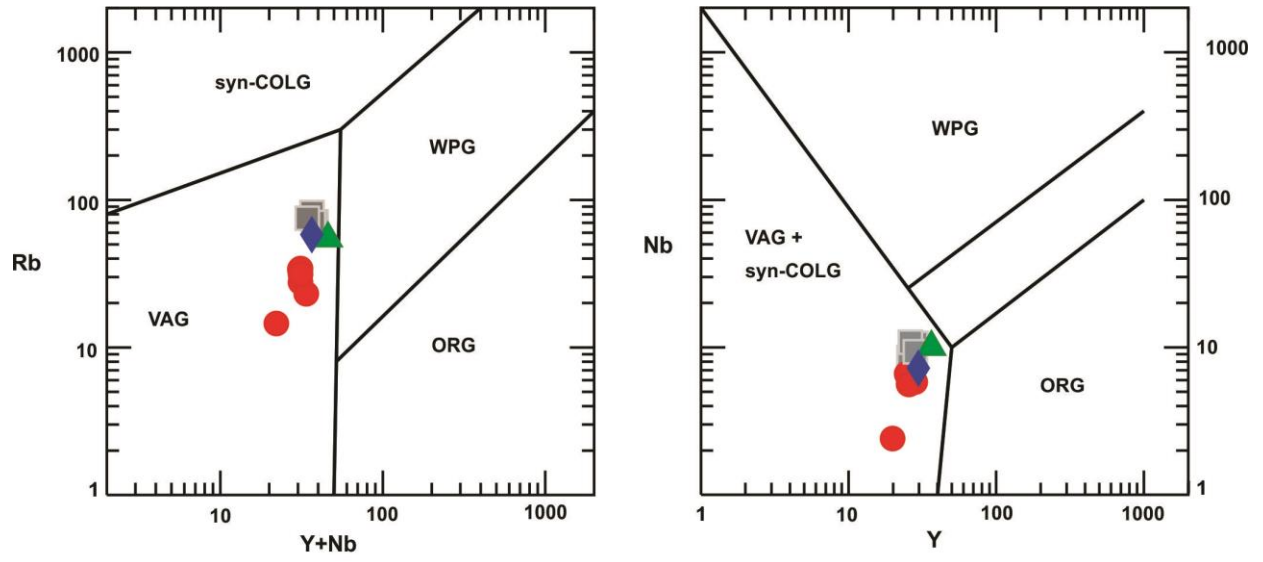


Figure 9

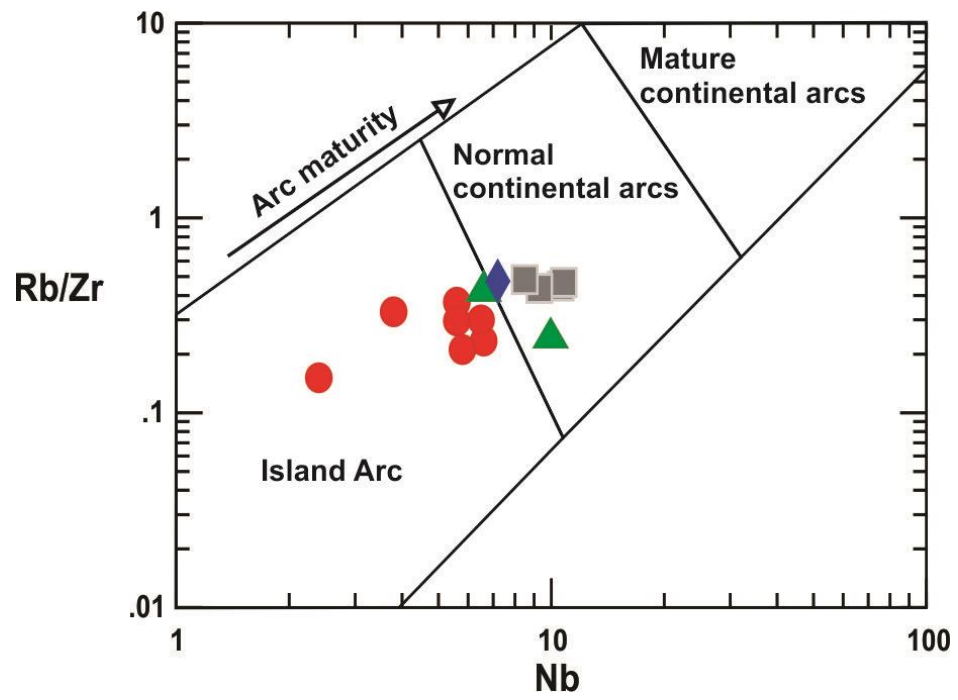


Figure 10

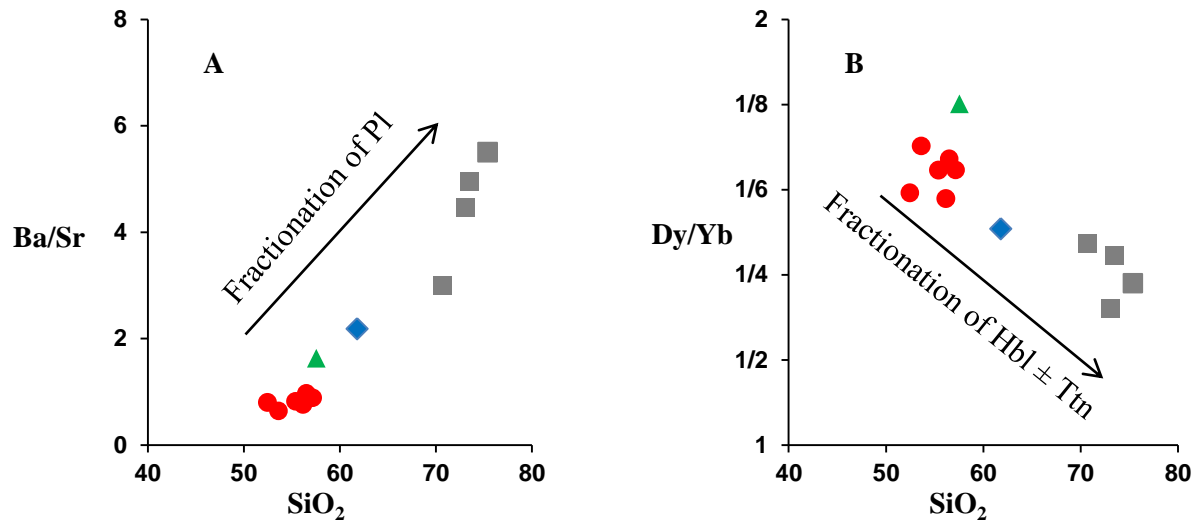


Figure 11

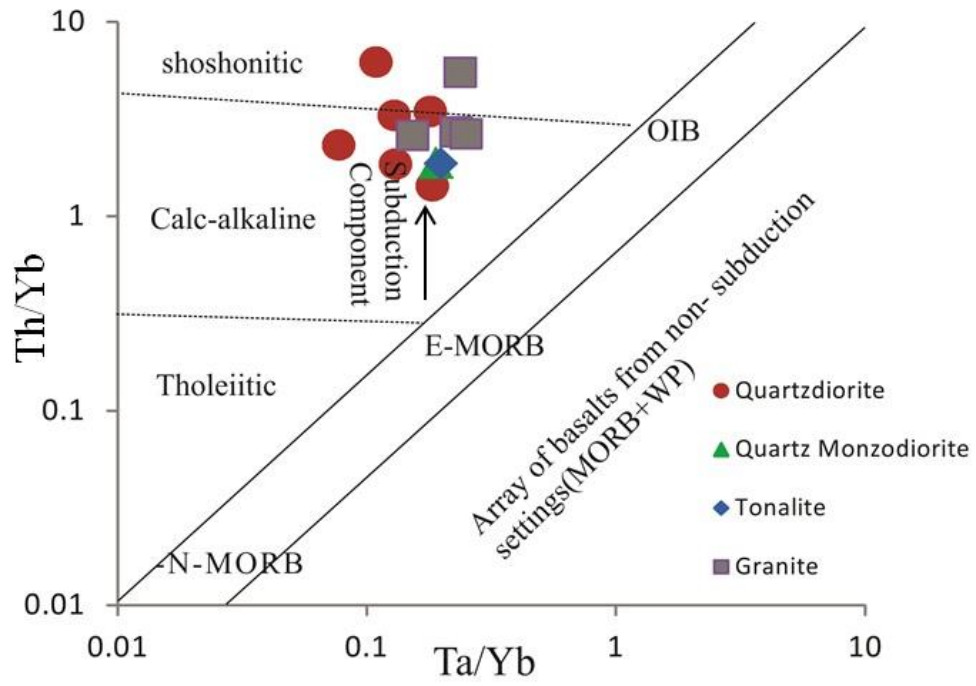


Figure 12

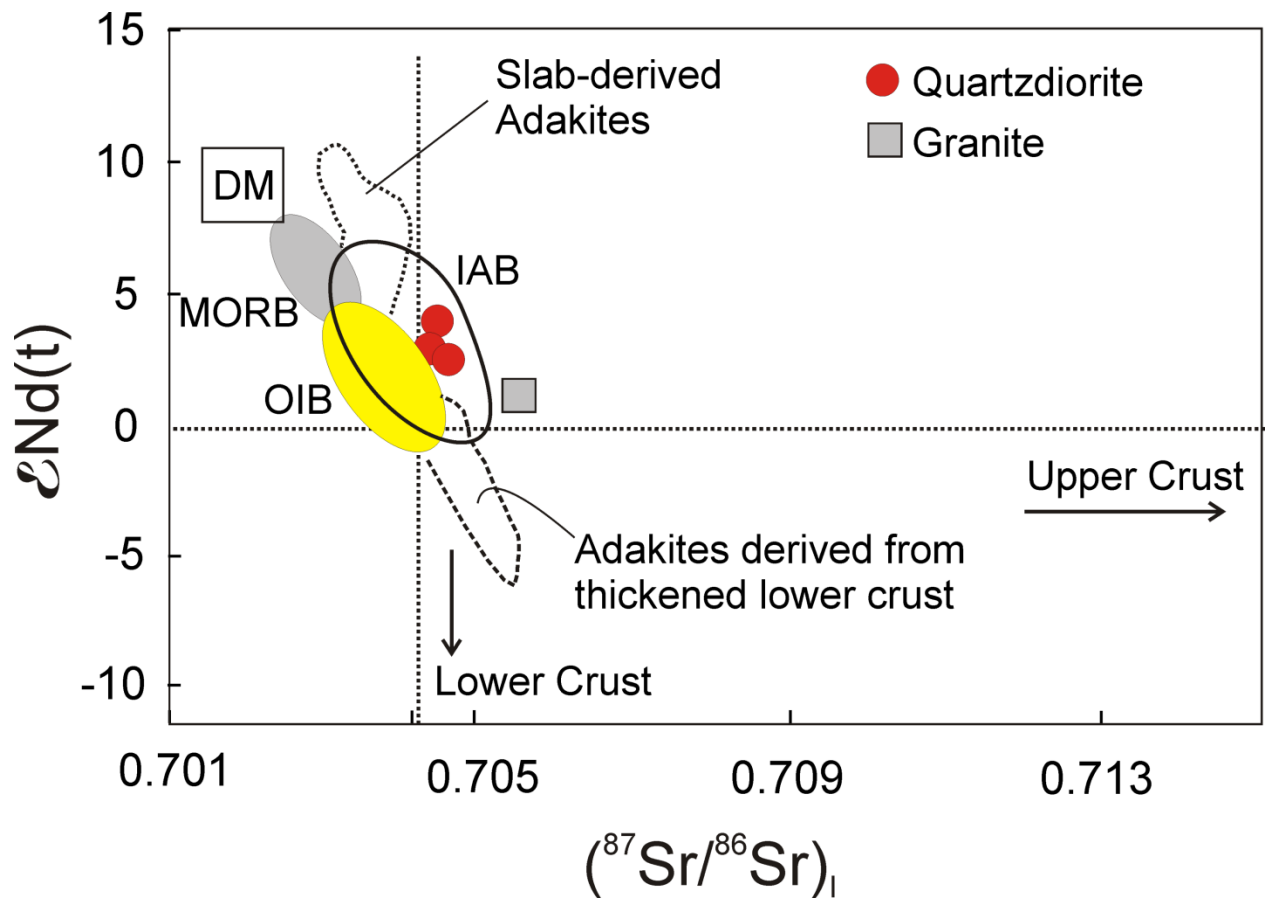


Figure 13